ANALYSIS OF THE EFFECTS CAUSED BY ALKALI AGGREGATE REACTION ON THE STRUCTURES OF MOXOTÓ POWER PLANT

Marco Juliani[1],* Alberto J. C. T. Cavalcanti[2], Ricardo Carrazedo[1], José C. Gaspare[3]

[1]Ieme Brasil Engenharia Consultiva Ltda
Rua MMDC, 499, SÃO PAULO, Brasil, CEP 05510-021.

[2]Companhia Hidro Elétrica do São Francisco – CHESF
Rua Delmiro Gouveia 333, RECIFE, Brasil, CEP 50761-901.

[3]Gana Consultoria e Engenharia
Rua Demóstenes 636, SÃO PAULO, Brasil, CEP 04614-139

Abstract

The Apolônio Sales (Moxotó) Power Plant, which is part of Paulo Afonso Hydroelectric Complex, was built between 1972 and 1977. Since the early stage of the commercial exploitation the units presented an abnormal performance with progressive shifting and tilting of the turbine shaft. The first visual evidences of alkali-aggregate reaction were several cracks noticed on walls and slabs in 1979. The cutting of 3 expansion slots between the concrete blocks, performed in 1988 - 1992 period, improved the performance of the generating units during some time. Meanwhile, the concrete expansion cumulated stresses and strains in the turbine parts fixed in the concrete, such as the stay vanes, the bottom and the discharge rings. To counteract these effects a rehabilitation process was implemented. This work presents the implementation and results of a numerical analysis developed using the FEM to evaluate the long term behavior of AAR in Moxotó Power Plant.

Keywords: Alkali aggregate reaction, numerical analysis, power plant, structural monitoring, remedial measures.

1 INTRODUCTION

Moxotó Hydro electrical Power Plant, which belongs to CHESF – Companhia Hidrelétrica do São Francisco is located in the São Francisco River, in the state of Alagoas, Brazil, immediately upstream to Paulo Afonso Hydroelectic Complex.

The Water Intake – Power Station concrete structures have a maximum 59,50m height and 30,50m wide blocks, totalizing a 122,00m length, plus an assembling area, and is equipped with 4 generating units of 110 MW driven by Kaplan Turbines. The construction began in 1972, having its reservoir been filled up in mid 1976. First generating unit started commercial operation in 1977. Since the early stage of the commercial exploitation, the units presented an abnormal performance with progressive shifting and tilting of the turbine shaft that finally lead to the rubbing of the blades on the discharge ring.

First evidences of alkali-aggregate reactivity - AAR - in Moxotó Plant date from 1979, i.e., only two years after Plant first operation, when a whole series of cracks on its walls and slabs had started to draw the attention of CHESF's technicians. An investigation program concluded that the cause of the problems was the Alkali-Silica Reaction due to the combination of granite aggregates and high alkali cement used in the construction.

The cutting of 3 expansion slots between the concrete blocks, performed during the 1988 - 1992 period, improved the performance of the generating units during some years [1] [2]. Meanwhile, the concrete expansion cumulated stresses and strains in the turbine parts fixed in the concrete, such as the stay vanes, the bottom and the discharge rings. To counteract these effects, a rehabilitation process was implemented.

The remedial measures started with the removal of the second stage concrete at the stay ring bottom side, and continued to the upper part of the draft tube. After the concrete removal, the stay vanes, discharge ring and lower lip plate became free to be displaced. A volume of about 130 m³ of concrete was removed.

The stress relief of the stay vanes was accomplished by cutting the rib base welds at their lower end. At the upper part of the stay ring, the vanes remained fixed to the concrete. After the complete

* Correspondence to: mjuliani@iemebrasil.com.br

release of the vane, the six base ribs were welded again taking care to minimize the heat-induced stresses [3].

Present studies deals with an analysis of effects caused by expansion reopening. This analysis was performed with mathematical models, developed with the software ANSYS – version 6.1. An iterative algorithm, which has enabled to consider the effect of concrete expansion along the service life of the power house, as well as viscoelastic effects in concrete was used.

2 INSTRUMENTATION AND LABORATORY TESTS

Concrete petrographic analysis showed that the aggregates in Moxotó have several lithologies, with mostly granite and biotite-gneiss. Basic composition was feldspar (60-65%), quartz (20-25%), biotite (5%), muscovite (5%) and chlorite / titanite / epidote / apatite / opaques (<5%) as secondary minerals. From the reactivity point of view, the presence of deformed quartz and alkaline feldspars (microcline), as potential reactive minerals, was detected.

Multiple extensometers were installed vertically and inclined from Moxotó Power Station Water Intake. Vertical wire extensometers were also installed, associated to inverted pendulums. These instruments are highlighted in Figure 1.

A reduction in concrete expansion rates was noticed, from the cutting of expansion slots between blocks (1988 to 1991) in an apparently permanent way. Water Intake multiple extensometers, for instance, that used to indicate an 80 με/year average concrete expansion rate before cutting, have revealed an approximate reduction to 50 με/year after slot cutting. Inverted pendulums, installed at the equipment wells vicinities, that used to indicate a vertical expansion rate around 70 με/year, have revealed a reduction to respectively 65 με/year during slot cutting and 45 με/year after cutting was performed. Expansion rates after cutting are, in mean terms, around 60% to 70% of previously observed rates.

3 MATHEMATICAL MODEL

The mathematical model comprises generating units GR1, GR2 and assembling area, as well as rock mass foundation and has 17343 nodes and 58587 elements. A symmetry plan between generating units GR2 and GR3 was used. Figure 2 allows visualization of the constructed model.

The following types of finite elements were used:

- SOLID 45 – with 8 nodes and three degrees of freedom per node for both the concrete and the rock mass elements;
- SHELL 63 – with 4 nodes and 6 degrees of freedom per node for turbine generator set elements;
- BEAM 4 – with 2 nodes and 3 degrees of freedom per node for turbine generator set elements.

Two expansion slots were considered in the model, being the first between generating units GR1 and GR2 (slot 1-2) and the second between generating units GR2 and GR3 (slot 2-3). By removing and replacing couplings of nodes in the slots areas the cutting, closing and reopening of the expansion slots were simulated.

3.1 Material properties

Material elastic properties are shown in Table 1. Elastic isotropic behavior was adopted for the whole model, as initial hypothesis.

3.2 Concrete expansion model

Concrete expansion rate (ε_0) variation with time (t) was determined from logarithmic regressions of measurements performed by inverted pendulums PI 2, 3 and 4. Figure 3 shows results of PI-3 inverted pendulum measurements results and respective equation generated by means of regression for this instrument.

Considering Inverted Pendulums 2, 3, and 4 results, the following equation was obtained:

$$\varepsilon_{0v} = 180 - 46 \ln t \qquad \text{(vertical expansion rate)} \qquad (1)$$

Above mentioned equation was used for $t \geq 3$ years. For t lower than 3 years, a linear increase for expansion rate was considered up to 130 με/year (obtained with the above equation for $t = 3$ years). The relation adopted between horizontal and vertical expansion rates was of 0.5.

The expansion rate (ε) was calculated as a function of the existing confining stress with the use of the following equation:

$$\varepsilon = \varepsilon_0 - K \cdot \log (S/So) \quad (2)$$

with:
ε = expansion rate (εx, εy, εz);
ε_0 = expansion rate without confining;
S_0 = stress below which expansion is constant;
S_u = stress above which expansion is null;
K = constant defined by the slope of the line that relates expansion to the logarithm of confining stress;
S = confining stress (Sx, Sy, Sz).

The relation between the expansion rate and the confining stress is graphically expressed in Figure 4. Adopted confining stresses were S_0 = 0,3 MPa and S_u = 4,0 MPa.

Error! Bookmark not defined.

3.3 Concrete viscoelastic behaviour

The alkali-aggregate reaction changes some concrete viscoelastic parameters, increasing both creep and stress relaxation, also reducing the elastic modulus with time. For the function concrete creep, the model adopted by the U.S. Bureau of Reclamation [4] was used:

$$f(k, t-k) = \frac{1}{E(k)} + F(k) \cdot \ln(1 + t - k) \quad (3)$$

with:
k = load application age
t = age for creep calculations

Since data on Moxotó concrete creep tests were not available, data from similar concrete types were used [5].

The following equation was adopted, in order to consider elastic modulus variation from load application date:

$$1/E\,(k) = 33.33 + 12.08 \log (k) \quad (4)$$

with k being the time in years and 1/E(k), given in 10^{-6}/MPa.

F(k) determination, from load application date, is given by:

$$F\,(k) = 3.177 + 9.526 \log k \quad (5)$$

with k being the time in years and F(k), given in 10^{-6}/MPa.

The relaxation curves were calculated for each year according to SOUZA LIMA et al. [6] [7]. Figure 5 presents adopted curves for 1/E(k), F(k) and the relaxation curve for k = 1 year.

3.4 Algorithm for time-dependent properties

An incremental procedure was used in order to enable time-dependent concrete properties: expansion rate, elastic modulus, creep and relaxation. Such procedure was divided into steps, one for each year of analysis as follows:

- 1st step (t=0): application of initial load, composed of concrete self weight, equipment weight and hydrostatic loads;
- 2nd step (t=1 year): calculation of the expansion rate (as function of initially applied load), elastic modulus, creep, and relaxation, calculation of stresses and displacements, considering all effects simultaneously;
- Step n+1 (t = n years): calculation of the expansion rate (as function of load applied in the year n-1), elastic modulus, creep and relaxation; calculation of stresses and displacements, considering all effects simultaneously.

3.5 Load application and boundary conditions

Boundary conditions were applied on model lateral and bottom faces, described as follows: Uz=0 on the vertical symmetry plan at the right face and on the vertical plan at the left face of the

model; Ux=0 on the vertical plan at the downstream and upstream faces; Ux=Uy=Uz=0 on the horizontal lower plan at the bottom of the model.

As acting forces, concrete and installed equipment self weights, hydrostatic loads (elevation 252,00m) and the stress relief due to the slot cutting were applied. Relief stresses due to slot cutting were applied with the opposite sign and with the same value of acting stresses (accumulated) in the year of cutting and considering the correspondent relaxation rate. Relief stresses on turbine stay vanes were applied with the opposite sign and with the same value of the acting stresses (accumulated) in the step corresponding to year of stress relieving operation. The whole period since end of construction up to 2014 was considered including the slot cutting and stress relieving operations.

4 RESULTS

4.1 Expansion rates

Measured expansion rates (EXP) were calculated based upon several instrument data and were then compared to the expansion rates obtained from the mathematical model (FEM). As it can be observed in Figures 6 and 7, a good correlation between measured expansion rates and the ones evaluated by the mathematical model was obtained. This way, the mathematical model was calibrated to predict the future expansion rates, considering either reopening or not of the expansion slots in 2004 (predicted behavior). It can be observed from results predicted by the mathematical model, that a reduction in the expansion rates is expected to occur until 2014, regardless of the slot cutting.

Additional data used for comparison with the mathematical model results were the leveling of topographical monuments on the water intake crest (MS-TA) and in the power station (MS-CF). The expansion rates referred to these instruments are presented in Figure 8.

4.2 Turbine cover unevenness

Table 2 presents obtained turbine unevenness values with the mathematical model. The 6,7mm unevenness, measured in the GR-2 unit in 1999, was very close to the one calculated by the mathematical model. The behavior was then predicted by the mathematical model until 2014, considering whether slots should or not be cut. It can be observed there was no significant difference in predicted turbine unevenness in 2014, regardless whether slot should or not be cut.

4.3 Stresses on stay vanes

Stresses on stay vanes, considering the hypotheses – of performing or not the slot cutting – were also evaluated. Figure 9 presents the stresses on both GR-1 and GR-2 stay vanes. It can be observed a significant reduction in the stresses in 1999 due the stress relieving operation. After these, stresses have not increased significantly until 2014, regardless of further slot cutting in 2004.

Figure 10 shows the evolution of stresses on units GR-1 and GR-2 most loaded stay vane. It can be again observed that stresses have not increased significantly after components disassembling and reassembling.

4.4 Circular cross-section ovalization

Ovalization in circular cross-sections of both generator and rotor chamber were evaluated, considering that, in 1999, components were disassembled and reassembled and that ovalization was eliminated this year. Cross-section ovalization index was calculated with the use of the following equation:

$$Iov = \frac{(F-f) \times 100}{D} \qquad (6)$$

with:
Iov = ovalization index in %;
F = Greater diametral gap;
f = diametral gap orthogonal to F;
D = nominal diametral gap;
D = 26 mm for generator air gap;
D = 12 mm for turbine rotor diametral gap.

The radial gap for both rotors and generators GR-1 and GR-2 were evaluated and are presented in Figure 11. In Figures 12 and 13 it can be observed that, after disassembling, the gaps were reestablished to their nominal values and have almost not increased in the subsequent period

until 2014, regardless of performing a further slot cutting in 2004. The same can be said about the ovalization index.

5 CONCLUSIONS

The mathematical model results have shown a good correlation to performed measurements with the instruments installed in the power house and was used to predict the behavior along subsequent years, by considering two hypotheses: performing – or not – a new cutting in the expansion slots in 2004.

The mathematical model has shown that, regardless of performing a further slot cutting in 2004:

- A reduction in expansion rate has occurred until 2014;
- Stresses on turbine stay vanes were of no concern, reaching values around 30 MPa until 2014;
- Turbine head cover unevenness calculated until 2014 was below 2 mm, being acceptable for operation;
- After disassembling components in 1999, turbine radial gaps hadn't reduced significantly and are not expected to do so until 2014;
- After disassembling components in 1999, ovalization index have gone up to only 10% until 2014.

Based upon above mentioned information, it can be concluded that further slot cutting planned for 2004 would not be necessary and the power house will be able to operate in acceptable conditions until 2014.

5.1 REFERENCES

[1] Silveira J. F. A., Degaspare J. C. Cavalcanti. (1989). "Investigations on the Moxoto powerhouse concrete affected by AAR". 8th International Conference on Alkali Agreggate Reaction. Kyoto. Japan.

[2] Silveira J. F. A., Degaspare J. C. Cavalcanti. (1989). "The opening of expantion joints at the Moxoto powerhouse to counteract the AAR". 8th International Conference on Alkali Agreggate Reaction . Kyoto. Japan.

[3] Cavalcanti A. J. C. T., Campos A. T., Silveira E. M. M., Wanderley E. G. (2000). "Rehabilitation of a generating unit affected by alkali-aggregate reaction." 11th Int. Conference on Alkali-Aggregate Reaction in Concrete. Quebec. Canada.

[4] U. S. Bureau of Reclamation. (1956) "Creep of concrete under high intensity loading". Concrete Laboratory Report N0 C-820, Denver, USA.

[5] Pacelli de Andrade W. (1997) "Concretos massa, estrutural, projetado e compactado com rolo – ensaios e propriedades."Editora Pini, São Paulo, Brasil.

[6] Souza Lima, V.M., Zagottis, D. E André, J. C. (1976) – "As Tensões de Origem Térmica nas Barragens e o Comportamento Viscoelástico do Concreto", XI Seminário Nacional de Grandes Barragens, Fortaleza, Brasil

[7] Souza Lima, V. M.; Guedes, Q. M.; Andrade, W. P. E Bastos, J. T. (1979) – "Cálculo da relaxação de Tensões a partir da fluência do Concreto". Revista Construção Pesada.

TABLE 1 – Materials elastic properties.

Material	Elastic Modulus (MPa)	Poisson's Rate	Specific Weight (kN/m³)
Rock Mass	15000	0.2	-
Concrete	30000	0.17	24
Steel	210000	0.3	78

TABLE 2 – Turbine cover unevenness – results obtained from the mathematical model.

YEAR	1999	2004	2014 with cutting	2014 without cutting
Calculated Unleveling (mm)	6.3	1	1.9	1.7

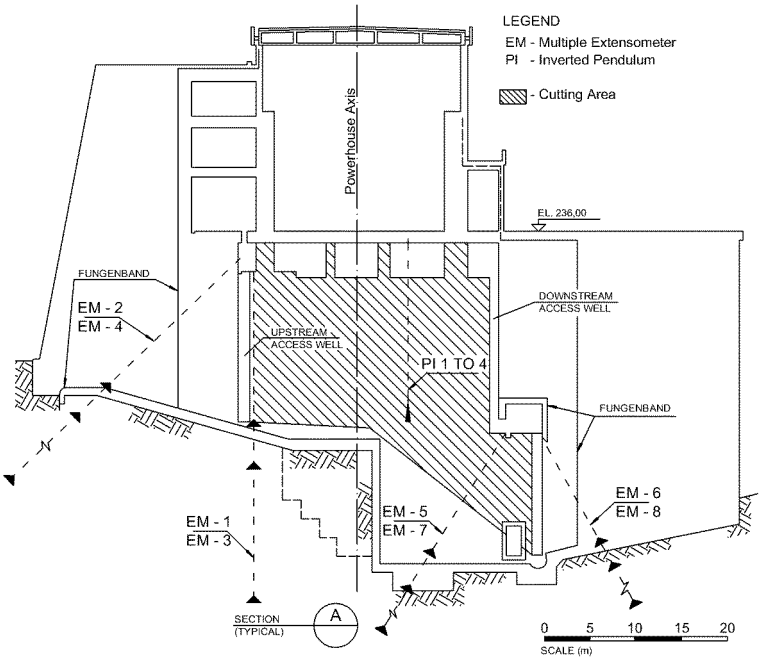

Figure 1: Instrumentation installed in the dam.

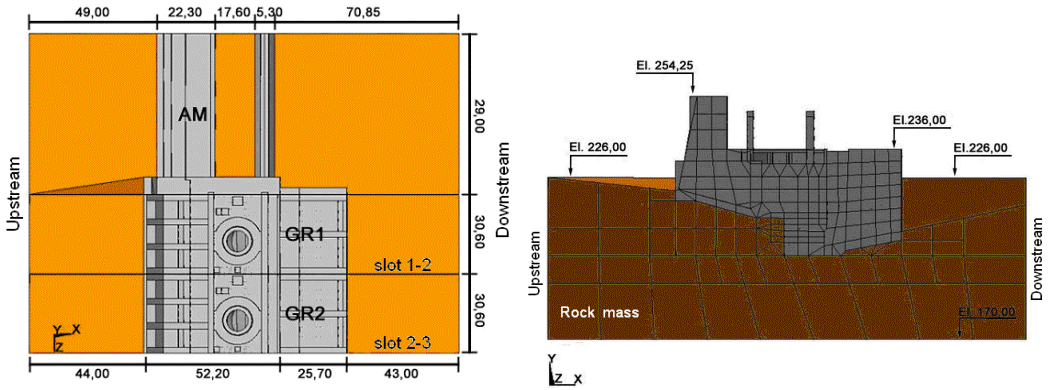

Model geometry plan view Model geometry side view

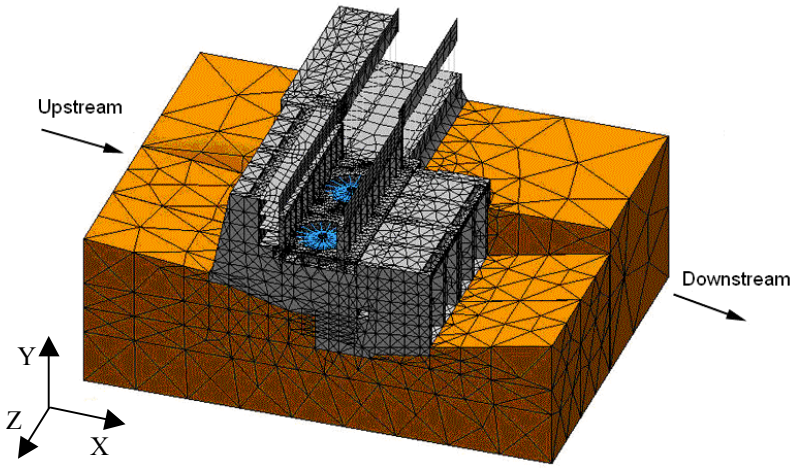

Mesh and model geometry perspective

Figure 2: Mathematical model geometry.

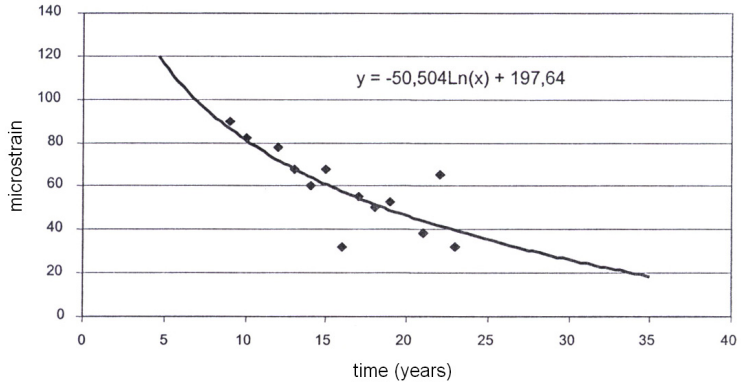

Figure 3: Expansion rate variation measured from PI-3.

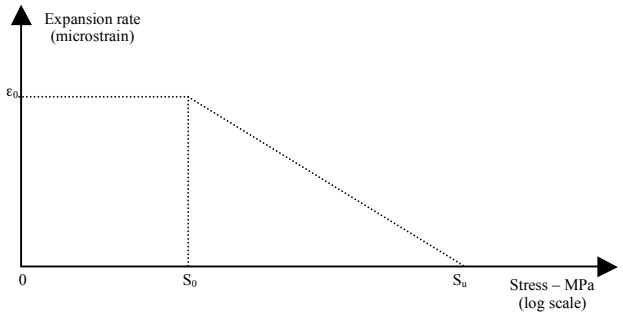

Figure 4: Relation between expansion rate and confining stress.

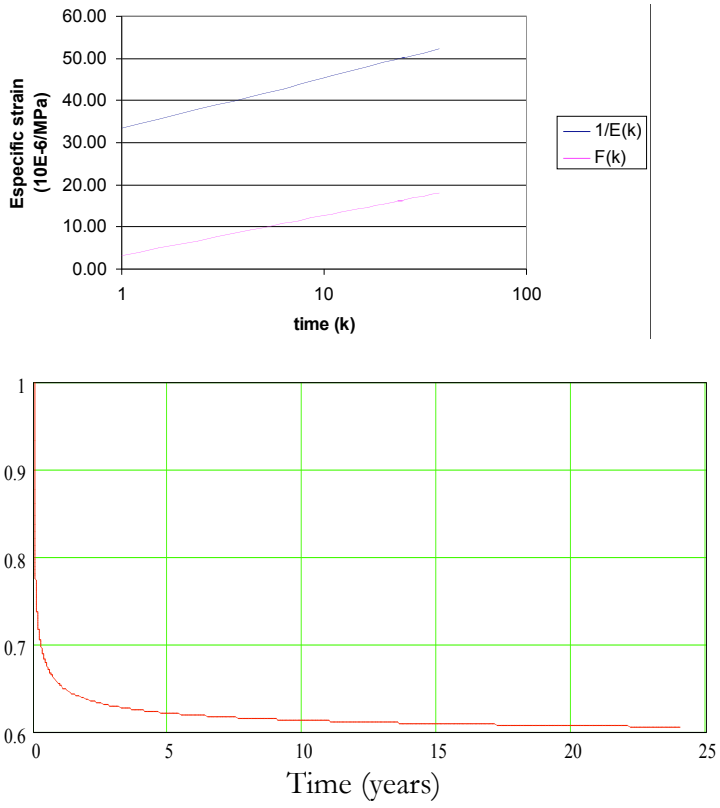

Figure 5: Functions 1/E(k), F(k) and relaxation curve.

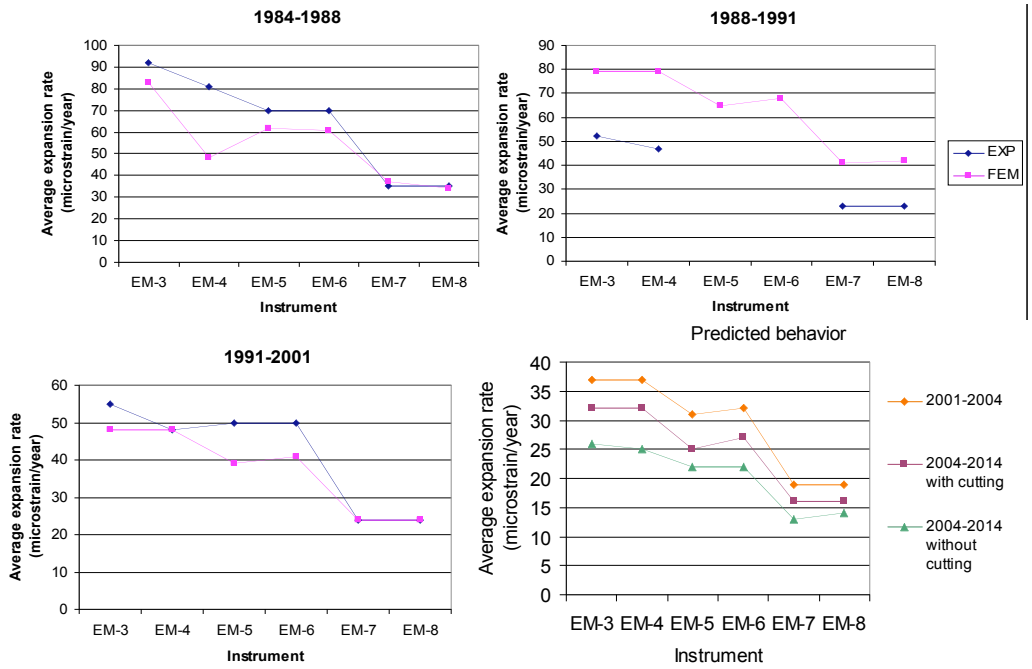

Figure 6: Expansion rates obtained with displacements measured by both the rod extensometers and the mathematical model.

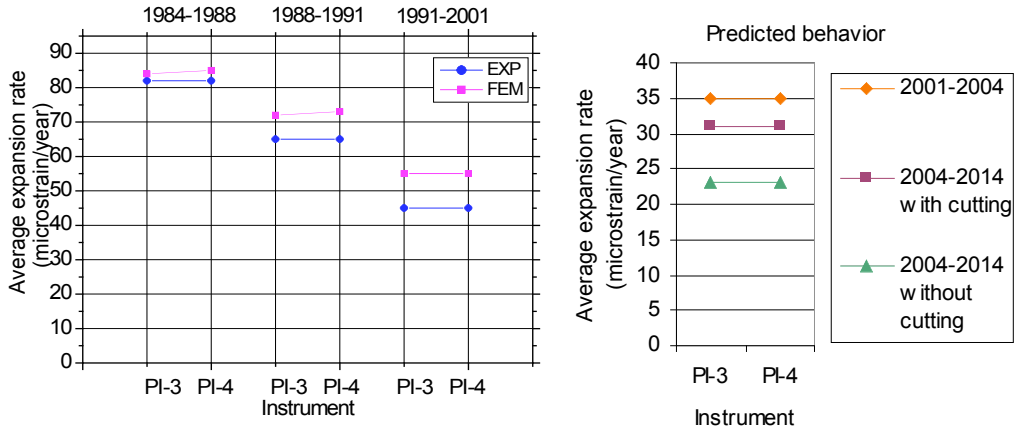

Figure 7: Expansion rates obtained with displacements measured by both the wire extensometers associated to inverted pendulums and the mathematical model.

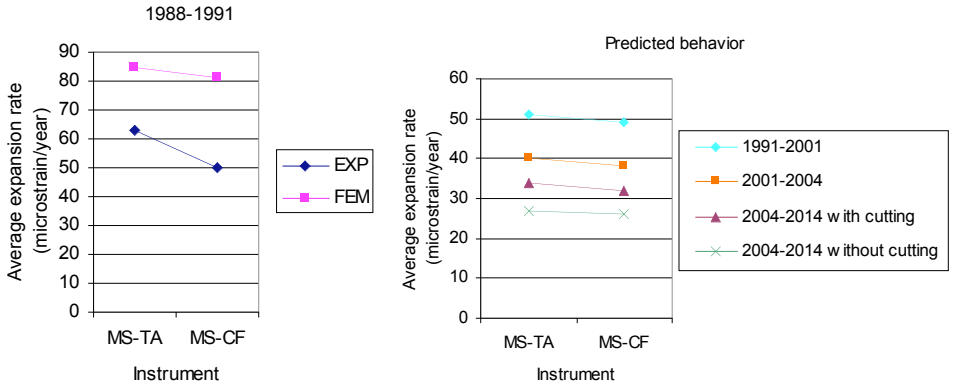

Figure 8: Expansion rates obtained with displacements measured with both the topographical monuments and the mathematical model.

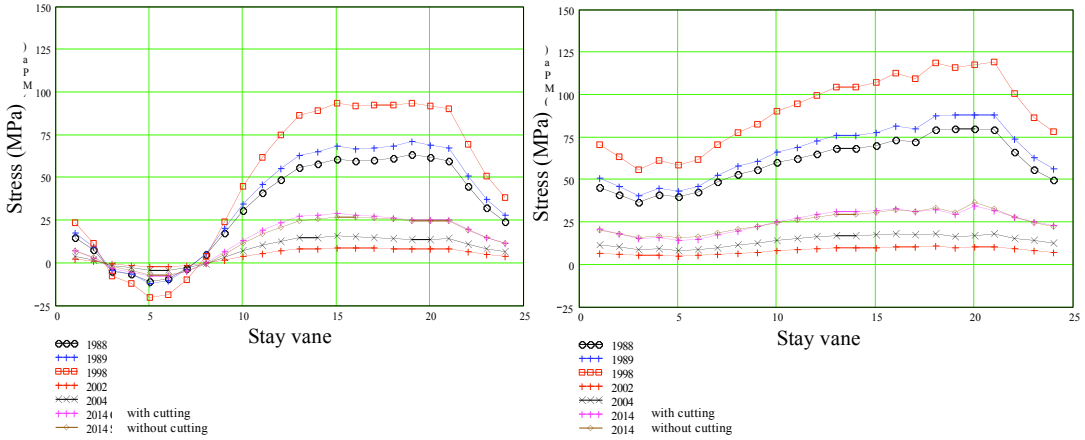

Figure 9: Stresses on stay vanes.

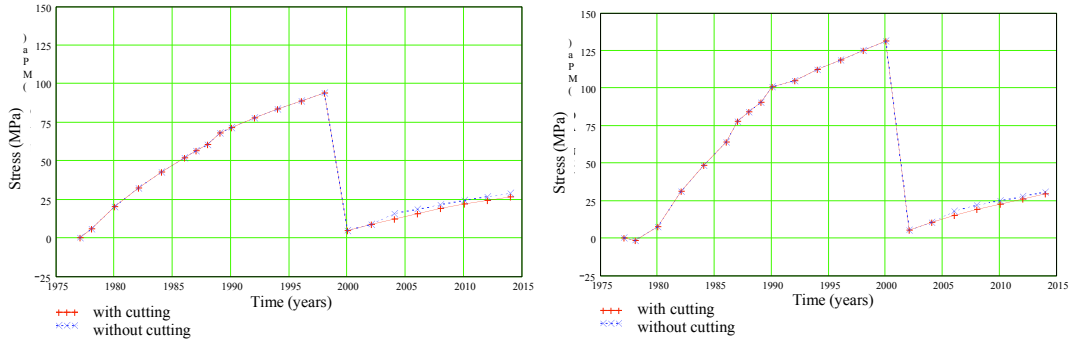

Figure 10: Most loaded stay vane stress evolution.

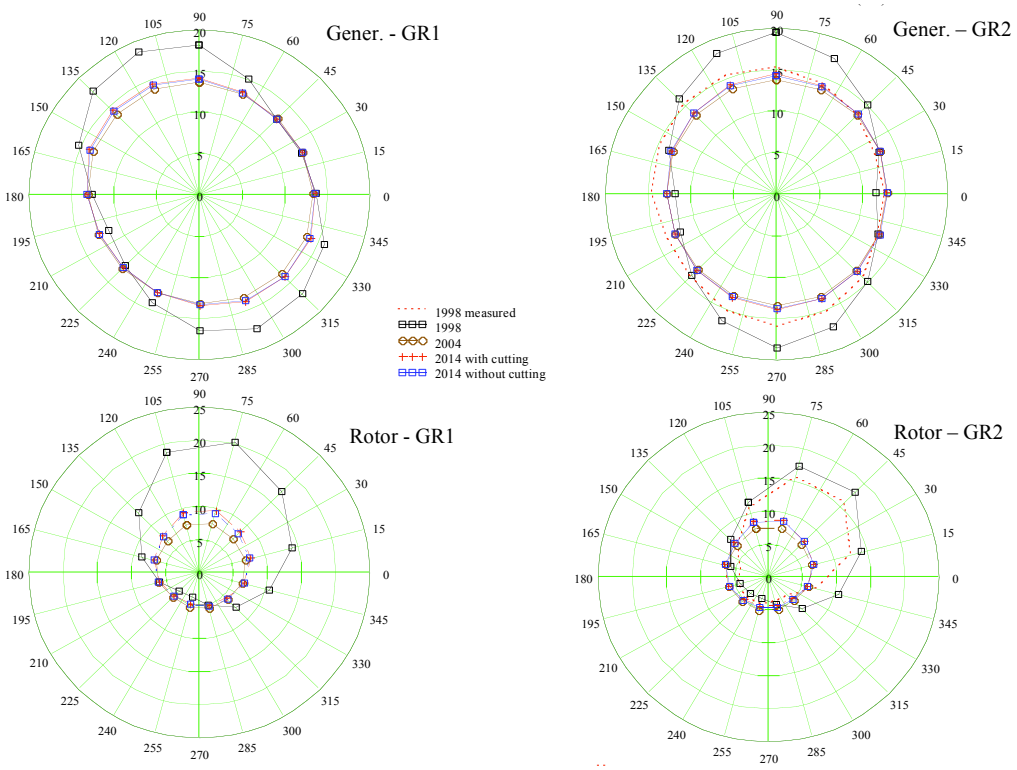

Figure 11: Radial gaps in rotors and generators.

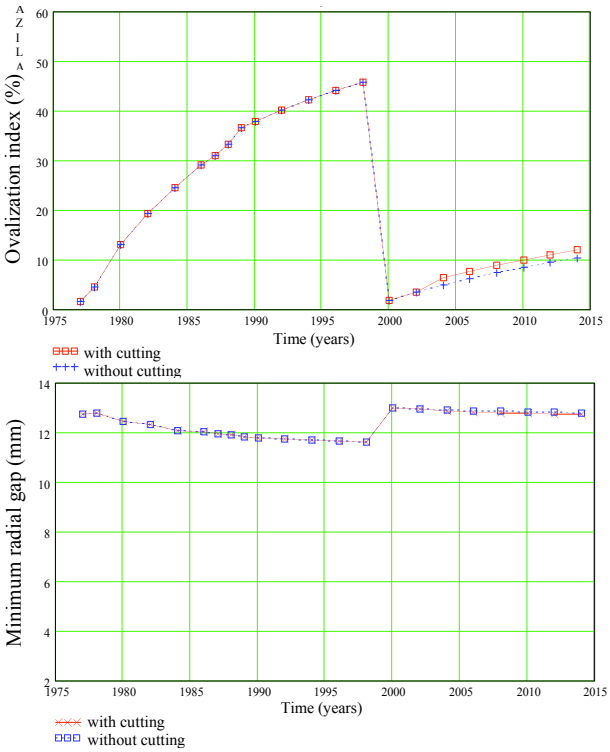

Figure 12: Evolution of ovalization index and minimal radial gap – GR1.

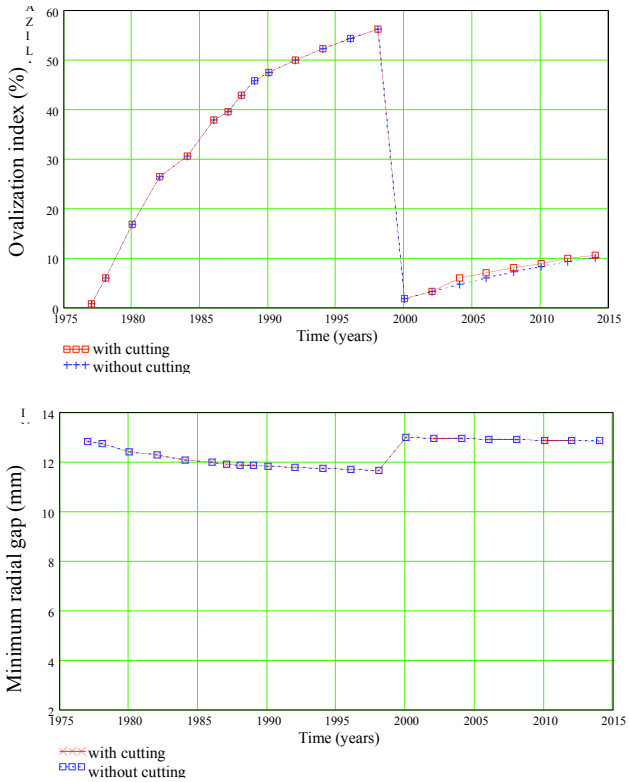

Figure 13: Evolution of ovalization index and minimum radial gap – GR2.